**Geomechanics and Engineering**, *Vol. 35, No. 5 (2023) 475-486*
https://doi.org/10.12989/gae.2023.35.5.475


# Effects of normal stress, shearing rate, PSD and sample size on behavior of ballast in direct shear tests using DEM simulation

Md Hussain*[1,2] and Syed Khaja Karimullah Hussaini[1a]

[1]*Department of Civil and Environmental Engineering, Indian Institute of Technology Patna, Bihar-801106, India*
[2]*Department of Civil Engineering, Saharsa College of Engineering, Saharsa, Bihar-852201, India*

(*Received November 22, 2022, Revised November 7, 2023, Accepted November 14, 2023*)

**Abstract.** Ballast particles have an irregular shape and are discrete in nature. Due to the discrete nature of ballast, it exhibits complex mechanical behaviour under loading conditions. The discrete element method (DEM) can model the behaviour of discrete particles under a multitude of loading conditions. DEM is used in this paper to simulate a series of three-dimensional direct shear tests in order to investigate the shear behaviour of railway ballast and its interaction at the microscopic level. Particle flow code in three dimension (PFC3D) models the irregular shape of ballast particles as clump particles. To investigate the influence of particle size distribution (PSD), real PSD of Indian railway ballast specification IRS:GE:1:2004, China high-speed rail (HSR) and French rail specifications are generated. PFC3D built-in linear contact model is used to simulate the interaction of ballast particles under various normal stresses, shearing rate and shear box sizes. The results indicate how shear resistance and volumetric changes in ballast assembly are affected by normal stress, shearing rate, PSD and shear box size. In addition to macroscopic behaviour, DEM represents the microscopic behaviour of ballast particles in the form of particle displacement at different stages of the shearing process.

**Keywords:** dilation angle; direct shear test; normal stress; particle displacement; particle size distribution; shear box

## 1. Introduction

Railways is most efficient, safe, and cost-effective mode of transportation in India and worldwide. Railways carry a large proportion of India's transportation. The Indian railway is the most extensively utilised means of public transportation for long and short distances in India and Nepal. The demand for efficient and high-speed rail (HSR) is rapidly increasing day by day due to rising population, rapid economic and industrial growth. The HSR requires a stable track structure. Ballasted rail track mainly consists of two-parts: structure and substructure.

Ballast is one of the key components of rail track (2017). It transmit and distribute the cyclic load to the sub-ballast and subgrade. Ballast absorbs vibration caused by high-speed train movement while also acting as a free draining component. Because of the such importance of ballast, numerous researchers have used laboratory testings to investigate the mechanical behaviour of railway ballast under static and cyclic loading. Large-scale triaxial, biaxial, pull-out test, box test, and direct shear tests are conventional laboratory tests (Wang *et al.* 2015). The direct shear test is a common and simple geotechnical engineering that is widely used to characterise granular matters such as soil and aggregate, particularly railway ballast (Tsoungui *et al.* 1999), Salazar *et al*. (2015), Liu *et al*. (2021), Indraratna *et al.* (2011a), Tsoungui *et al*. (1999).

For granular matters, studies based on traditional laboratory testing present results at the macroscopic level. The micromechanical implications of granular material's packing and shear characteristics are still unclear (Gong *et al.* 2021). Since ballast is discrete in nature, research using continuum approaches such as finite element analysis or finite difference analysis fail to capture the actual discrete behaviour of ballast (Ngamkhanong *et al.* 2017). On the other hand, the laboratory test findings do not provide microscopic characteristics of granular material assembly. Cundall and Strack (1979) has evolved discrete element method as a powerful tool for analysing discrete behaviour of granular matter. The behaviour of dense ($e$ = 0.18) and loose ($e$ = 0.24) PVC cylinder assembly was studied by Masson and Martinez (2001). Dilatant behaviour was observed in dense samples and contracting behaviour in loose samples. Cui and O'sullivan (2006) used steel spheres as an idealised material to analyze the micro-mechanics of direct shear tests in 3$D$ for granular materials. Based on inter-particle friction, they proposed a hypothesis for the discrepancy in simulation and laboratory results but did not accounted particle shape and angularity. for granular matter's shear behaviour is affected by particle shape. Huang *et al.* (2009b), Huang and Tutumluer (2011) and Huang and Tutumluer (2014) used laboratory and DEM modelling to study the shear behaviour of fresh and fouled ballast under direct shear loading. The University of Illinois Aggregate Image Analyzer (UIAIA) apparatus was used to model ballast DEM models, which captures the shape of the ballast particle. They observed that as fouling increases, ballast shear strength decreases. Indraratna *et al*. (2014),

*Corresponding author, Assistant Professor
E-mail: md.pce16@iitp.ac.in
[a]Assistant Professor
E-mail: hussaini@iitp.ac.in



ISSN: 2005-307X (Print), 2092-6219 (Online)

Wang *et al.* (2015) investigated the shear behaviour of ballast with the help of DEM simulation of large scale direct shear test. They employed PFC3D to simulate direct shear tests in DEM and used PFC3D clump logic to model the irregular shape of ballast particles. Indraratna *et al.* (2014) observed that DEM model indicates coal fines reduces shear stress and increases dilation of coal fouled ballast. It was shown that volumetric dilation predicted by DEM somewhat higher than measured in laboratory. Angularity, flakiness, elongation, and breakage of ballast were not considered by Indraratna *et al.* (2014) in their DEM simulation. The nonlinear response of ballast with normal stress was observed by Wang *et al.* (2015). They also observed that ballast with a broader gradation has higher shear strength. Wang *et al.* (2015) also observed increase in peak angle of shear resistance with contact friction coefficient. They concluded that coordination number increases with shearing process at large stress. Ngo *et al.* (2014) investigated a series of DEM simulations of direct shear tests for geogrid reinforced ballast behaviour combined with coal foul. Ballast and geogrid were modelled in DEM as clump in PFC3D. They observed that the interlocking of geogrid and ballast had an influence on the assembly's shear strength using the DEM direct shear test. Based on DEM results they concluded that strains develop non-uniformly across geogrod and magnitude of strain depends upon interlocking between geogrid and ballast. Suhr and Six (2016) examined the stress dependency of granular matter. They used experimental direct shear tests on single and paired glass beads to corroborate their findings. They observed normal stress dependency of bulk friction coefficient in experiment and explained normal stress dependency on inter particle friction in simulation. Suhr and Six (2017) conducted DEM simulation of cyclic compression and direct shear test for crushed rock.They observed that modelling ballast as a relatively simple geometry of two spheres together can produce DEM results that are similar to the experimental results. Suhr *et al.* (2018) compared the two types of railway ballast under cyclic compression and direct shear tests in DEM. They stated that if simple particle shapes are used, the conical damage model (CDM) is a preferable alternative for the simulation of railway ballast.

The shear behaviour of granular material is also affected by specimen size and shape in terms of peak shear strength and friction angle in the plane containing major or minor principal stress. An improper mechanical state of shear box causes stress-strain behaviour to become more non-uniform, which can have a major impact on the measured strength and dilatant characteristics (Mikasa (1960), Jewell (1989), Shibuya *et al.* (1997), Wu *et al.* (2008)). For large-scale testing, direct shear tests have been carried out on a variety of soil types using various specimen sizes in boxes with sizes ranging from (60 × 60 mm2) to more than (1000 × 1000 mm2). More research is required to examine the impact of the scale factor on the shear strength characteristics of the test samples because the change in shear box size, particularly for samples with large particles, lead to varied findings for the same tested sample (Zahran and Naggar 2020). In the past, many researchers have investigated the effects of size and shape of shear box on peak shear strength, deformation, friction angle and dilation characteristics of different types of soil. Parsons (1936) tested ottwa and crushed quartz in three shear boxes of size 36, 120 and 240 cm2 and found a slight decrease in peak frictional angle with an increase in shear box size. Carroll (1979) tested two clay samples using two circular direct shear test apparatus of diameter 40.6 and 80 mm under static and cyclic conditions. They observed that 10%−15% increase in shear strength with increase in shear box size for static condition while twice in cyclic condition. Palmeira and Milligan (1991) tested Llieghton and buzzered sand found no difference in frictional angle with an increase in shear box size. They also observed that peak shear strength increases with decreasing size of the shear box and the smaller shear box has the highest peak shear strength. Cerato and Lutenegger (2006) and Dadkhah *et al.* (2010) conducted series of direct shear tests on sand and clay with different specimen size and normal stress. They observed increase in angle of internal friction with decreasing shear box size.

From extensive literature review, it was observed that many researchers have conducted experimental and numerical simulation to examine the shear behaviour of ballast using large scale direct shear test at single normal stress and shearing rate. In practice, a rail track under operating conditions may be subjected to different shearing rates depending on the magnitude of cyclic stress and the train speed (Sweta and Hussaini 2019). However, there is no comprehensively reported literature that illustrates the effect of normal stress and shearing rate (representing the real track environment) using DEM simulation on the shear behaviour of ballast. Further, it was seen that the influence of shear box size has been investigated for soil but in case of railway ballast it has not been studied yet. Moreover, the particle displacement at different stages of shearing process has not been studied so far. Therefore, in the present study, the shear behaviour of ballast at different normal stress, shearing rate and specimen size are investigated at microscopic level using DEM simulation. Further, five different ballast gradations of three countries are considered in the study to see the effect of particle gradation on the behaviour of ballast. There are seven sections in this paper. Previous works are presented in section 1. The irregular shape of the ballast and shear box has been modelled in section 2. The shear behaviour of ballast at different normal loads is described in section 3. Section 4 investigate the effects of shearing rate. Section 5 discusses the impact of particle size distribution on ballast shear behaviour. In section 6, the influence of shear box size and shape is investigated. Summary and concluding remarks are given in section 7.

## 2. DEM simulation

The particle flow code (PFC3D) in three dimensions was developed using the discrete element approach (DEM) (Itasca 2017). PFC3D is capable of capturing the discrete be- haviour of granular particle assembly. The calculation cycle in PFC3D is a time-stepping algorithm that calculates contact forces and updates displacement in two cycles using New- ton's laws of motion. Contacts are updated from

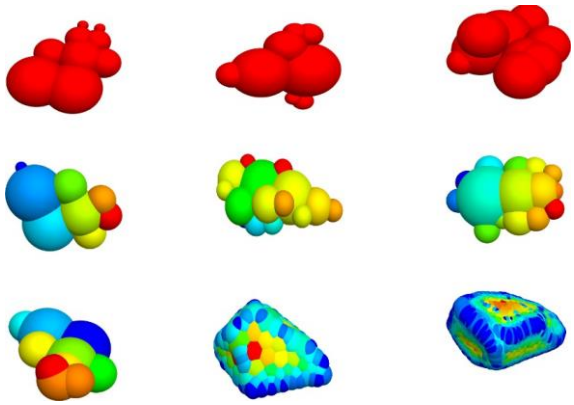

Fig. 1 DEM model for different shapes of ballast particle

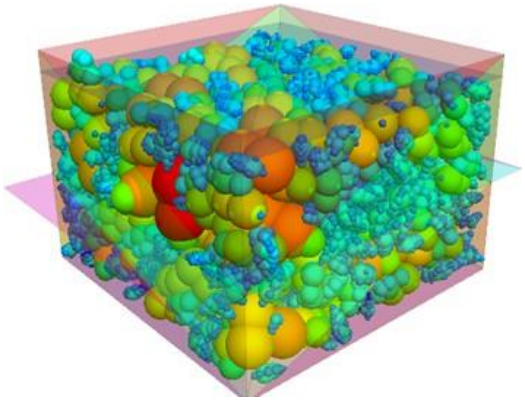

Fig. 2 Initial assembly of ballast in large-scale direct shear test

particle and entity positions at the start of each timestep. After that, the force-displacement law is applied to each contact in order to update contact forces based on relative motion between entities and the contact constitutive model. The law of motion is then applied to each particle based on the contact force, which creates a moment to update particle velocity and position.

### *2.1 Modelling of ballast assembly in DEM*

Ballast particles are irregular in shape and discrete in nature. It is difficult and inaccurate to model ballast as continuum material. To model discrete elements, PFC3D has three entities: wall, ball, and clump. In PFC3D, a spherical particle is represented by the ball entity. Due to insufficient interlocking and excessive rolling , spherical particles are unable to represent ballast particles (Oda and Iwashita 2020). Many researchers Lim and McDowell (2005), Lu and McDowell (2007), Indraratna *et al.* (2014), Wang *et al.* (2015) and Liu *et al.* (2021) have attempted to model the irregular shape of ballast using clump logic in PFC by overlapping several sized balls. These balls are arranged in such a manner that imitate the irregular shape of ballast particles by fixing coordinates of individual balls. As shown in Fig. 1, a subroutine in the FISH scripting language is created to generate particle templates of nine sample ballast models. A 300 mm ×300 mm ×190 mm large-scale direct shear box is modelled. The lower box is 90 mm high, While the upper box is 100 mm high, with the two boxes separated horizontally. A free loading plate is placed on top to uniformly apply normal load on the particles. The top plate's vertical displacement is useful for recording particle dilation effects as the shearing process progresses. The lower box can be moved while the upper box remains stationary. The DEM model of a large-scale direct shear box is shown in Fig. 2. The shear box is then filled with clump particles. The particle size distribution of IRS-GE-1 (2004) is used to generate ballast model particles, as shown in Fig. 3. The simulation of PSD of ballast is performed in two steps. First, a table containing the data from the sieve analysis as per the PSD adapted for laboratory tests is created in FISH. A domain is then created prior to the generation of clumps. To create the specimen as per the actual PSD, clumps are distributed in five bins inside box to match target porosity and particle size distribution without regard to overlapping of particles. These five bins are defined based on a range of sieve size and volume fractions.

To simulate experimental conditions, the ballast model particles are distributed with random orientation. The initial condition of the particles is controlled by setting the assembly porosity to 40%, which corresponds to a void ratio of 0.67. The void ratio 0*,* 67 is corresponds to field density of loosely placed ballast in the range of 1470−1550 $kg/m^3$ (Indraratna *et al.* 2013, Sweta and Hussaini 2018). The material modeling support in PFC Itasca (2017) provides material generation method and its behaviour with

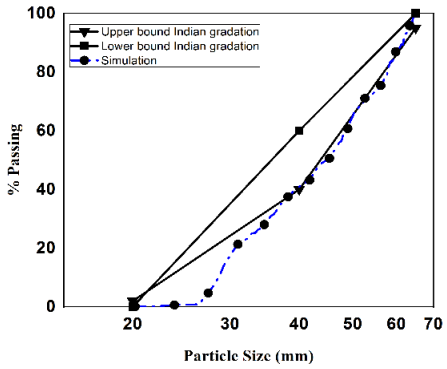


Fig. 3 Particle size distribution as per IRS:GE:1:2004

Table 1 Micromechanical properties adopted for ballast assembly and shear box

| Parameters | Values |
|---|---|
| Shear box dimension | 300 *mm* ×300 *mm* ×190 *mm* |
| Contact normal stiffness *(N/m)* | $0.52 \times 10^8$ |
| Contact shear stiffness *(N/m)* | $0.52 \times 10^8$ |
| Contact normal stiffness (particle-wall) *(N/m)* | $2 \times 10^8$ |
| Contact sheer stiffness (particle-wall) *(N/m)* Inter-particle friction coefficient (particle-wall) | $2 \times 10^8$ 0.5 |
| Particle density *(kg/m$^3$)* | 2700 |
| Damping ratio | 0.7 |

micro-structural properties. PFC provides in-built contact models such as linear contact models to simulate constitutive mechanical behaviour of material. In this study, a linear contact model is assigned using **CMAT** command in PFC. The DEM parameters used in the current study were adapted by conducting calibration of clump assembly subjected to a large-scale direct shear test with experimental data reported by Indraratna *et al.* (2011a). Based on it a set of micromechanical parameters adapted for DEM simulation of ballast are given in Table 1. Similar DEM parameters were also used by numerous researches (Wang *et al.* (2015), Indraratna *et al.* (2014), McDowell *et al.* (2006), Lim and McDowell (2005) for DEM simulation of ballast. The researchers have also calibrated and validated DEM model with experimental test results and found a good agreement.

After that, the assembly is cycled to reach equilibrium based on average ratio of unbal- anced and balanced forces. Then using the PFC3D's servo control mechanism, a constant normal load is applied to the top plate throughout the simulation, mimicking laboratory conditions. By assigning the lower box velocity to $1.66 \times 10^{-3}$ m/sec, the shearing rate of the test is achieved at 10 mm/min. The simulation uses a timestep of $1.6 \times 10^{-7}$. During the simulation process, a subroutine in FISH is developed to record the shear stress, shear displacement, and vertical dilation.

## 3. Influence of normal stress

The demand for heavy trains for freight transportation is rapidly increasing due to its safety, economy, and accessibility. Heavier trains apply high level of stress on the track and its components. The normal stress acting on operating track is depend upon axle load, track confining pressure and loading frequency (Sweta and Hussaini (2019)). Sweta and Hussaini (2019) determined the normal stress values for both loaded and unloaded track ranging from 64 kPa to 192 kPa. Wang *et al.* (2015) and Huang *et al.* (2009a) are analyzed ballast subjected to higher normal stress of more than 300 kPa. In this study, ballast is subjected to five different normal stresses of 35 kPa, 70 kPa, 140 kPa, 210 kPa and 280 kPa in DEM models of large scale direct shear tests. As indicated in Fig. 3, PSD is simulated between the upper and lower bound gradation of ballast as per IRS-GE-1 (2004). The variation of shear stress and volumetric strain are monitored during the shearing process. The peak dilation angle is computed as the inverse of the tangent of the ratio of the fraction of changes in vertical and shear displacements (Bolton 1986, Alam and Hussaini 2023). Fig. 4 shows the shear stress-shear displacement curve of ballast, which shows an increase in peak shear strength with increasing applied normal stress.

The increase in the applied normal stress results in the higher shear strength and den- sification of the ballast assembly. The densification of the ballast assembly results in the decrease in void ratio and increase in the interlocking of the ballast assembly. The decrease in void ratio with increased interlocking directly affect the drainage characteristics of ballast layer on railway track. It has been observed that among the five normal stress tests, there is a sudden drop in shear strength between 25 mm to 35 mm horizontal displacement. Ballast degradation appears to begin in this region of horizontal displacement. Within this range, particles in the upper box attempt to move toward the loading plate, while particles in the lower box move in the direction of shearing as shown in Fig. 6. Due to the upward movement of particles in upper box, particles breakage take place. It is also observed that the breakage of the ballast particles take place after 25 mm horizontal displacement. Uptil this range of horizontal displacement, the ballast particle mobilize and moved toward the upper box.

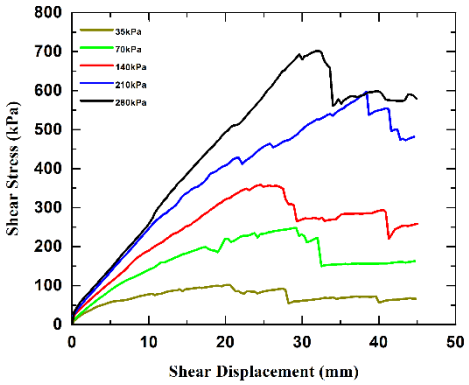


Fig. 4 Influence of normal stress on shear strength of ballast assembly

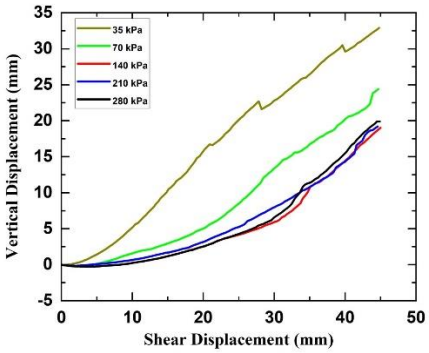


Fig. 5 Influence of normal stress on shear strength of ballast assembly

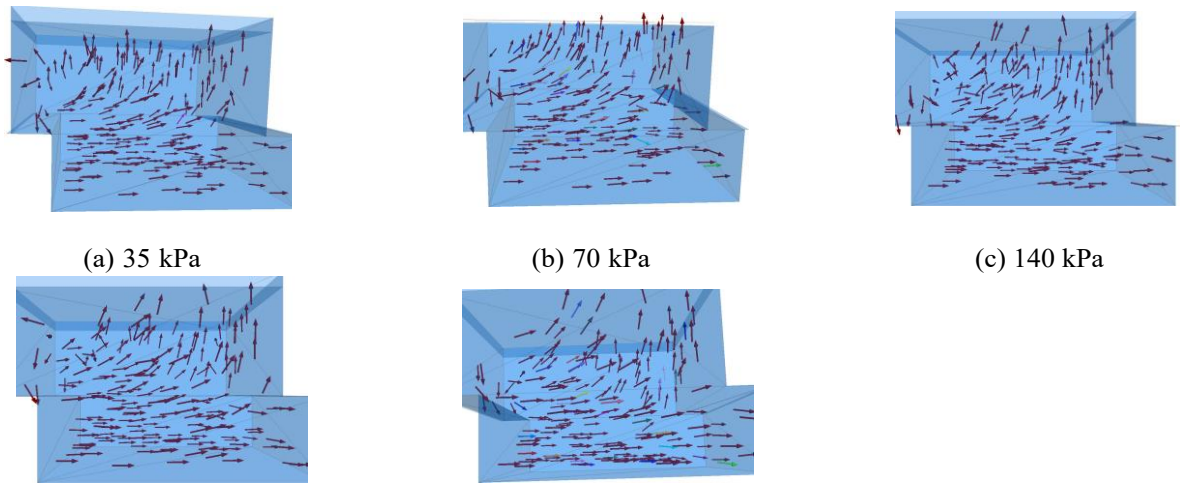

(a) 35 kPa (b) 70 kPa (c) 140 kPa

(d) 210 kPa (e) 280 kPa

Fig. 6 Ballast particle displacement at end of shearing at different normal stresses

The vertical displacement of the loading plate exhibits the dilation behaviour of ballast in the DEM simulation as shown in Fig. 5. The amount of dilation of ballast assembly is higher for low normal stress. At 35 kPa normal stress assembly dilates up to 33 mm. However, at 280 kPa normal stress value assembly dilates only 19 mm 2. The dilation angle of assembly is higher at low normal stress 2. The degradation of ballast particles reduces the strength of the ballast assembly, causing compression of the loading plate, followed by an increase in dilation with progress in shearing. At low normal stress, particles have a short range of elastic deformation and a broader range of plastic deformation. The plastic deformation increases with increasing normal stress. It indicates that at higher levels of compaction, ballast particles show plastic-like behaviour. The plastic deformation in ballast assembly causes plastic strain, which is one of main reasons of ballast degradation on track substructure. The rate of dilation is large at low

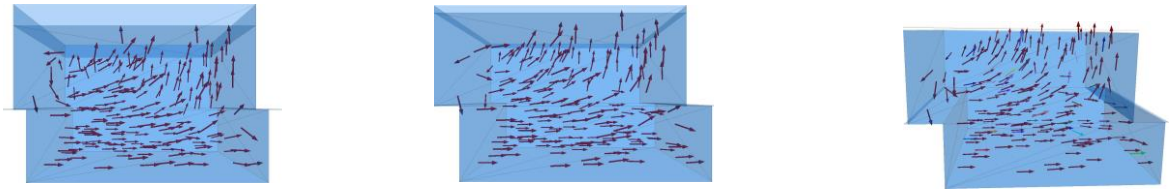

(a) 15 mm (b) 30 mm (c) 45 mm

Fig. 7 Ballast particle displacement during different stages of shearing at 70 kPa normal stresses

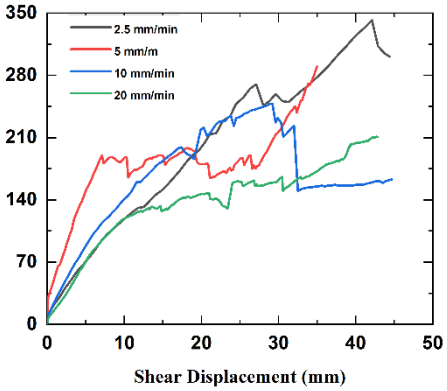


Fig. 8 Influence of normal stress on shear strength of ballast assembly

Table 2 Variation of shear strength parameters with normal stress

| Normal stress (kPa) | 35 | 70 | 140 | 210 | 280 |
|---|---|---|---|---|---|
| Peak shear stress (kPa) | 102 | 248 | 348 | 598 | 702 |
| Max. vertical displacement (mm) | 33 | 24.4 | 19.03 | 19.2 | 19.9 |
| Peak dilation angle (degree) | 21 | 18 | 15.3 | 11 | 9 |

normal stress than at high normal stress. At low normal stress, the ballast assembly densifies less and the ballast particles are more able to displace towards the vertical direction; causing vertical displacement of the loading plate. DEM captures this micro-mechanical behaviour of particles during the shearing process as shown in Fig. 7.

DEM models capture the particle displacement during the shearing process. Fig. 7 shows the particle displacement at 15 mm, 30 mm and 45 mm shear displacement. At 15 mm shear displacement, particles in the lower box displace horizontally, whereas particles in the upper box displace horizontally with some particles displaced downward, causing ballast assembly densification. As the shearing process progresses, particles in the upper box begin to displace diagonally upward, while particles in the lower box continue to displace horizontally. At the end of shearing process, upper box particles displace in the upward direction. Continum mechanics and laboratory experiments are unable to capture this micromechanical behavior.

## 4. Influence of shearing rate

The demand of high speed rail is rapidly increasing in India. It is a well known fact that high speed of trains causes high cyclic stress, shearing load and large ground vibration (Fu and Wu 2019). Qualitatively high shearing rate represents greater train speed (Sweta and Hussaini 2019).

Sweta and Hussaini (2019) computed the shearing rate corresponding train speed based on shear strain, length of shear plane and loading time. They computed shearing rate for loading frequency 10, 20 and 30 Hz (train speed 70-210 km/h) and axle spacing 2.02 m about 8.11 to 18 mm/min. Therefore, in this study four value of shearing rate 2.5, 5, 10 and 20 mm/min are selected to simulate ballast subjected to train speed upto 250 km/h.

The variation of shear stress with shear displacement at four different shearing rates 2.5, 5, 10, and 20 mm/min is shown in Fig. 8. The shear strength of ballast assembly decreases with increasing shearing rate. Peak shear stress decreases from 342 to 210 kPa as shearing rate increases from 2.5 to 20 mm/min. The variation of shear stress with shearing rate is nonlinear as shown in Fig. 11. A relationship is established as indicated in (1) peak shear stress with shearing rate. The values of empirical constants are $a$ = 63.19 and $b$ = 396.1. It can be seen from Fig. 8 stiffness of ballast assembly is high at low shearing rate and it decreases with increasing shearing rate. According to Fig. 9, at high shearing rates, there is a dramatic decline in shear stress in the 20 to 25 mm range of shear displacement. It appears to be caused by ballast breaking, and greater

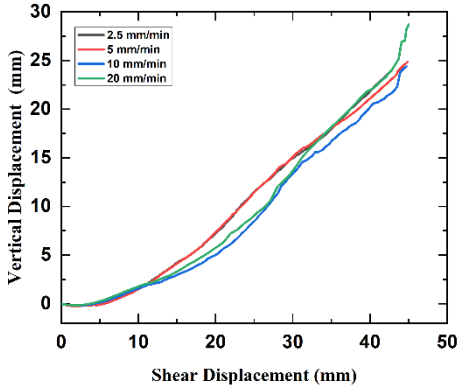


Fig. 9 Influence of normal stress on shear strength of ballast assembly

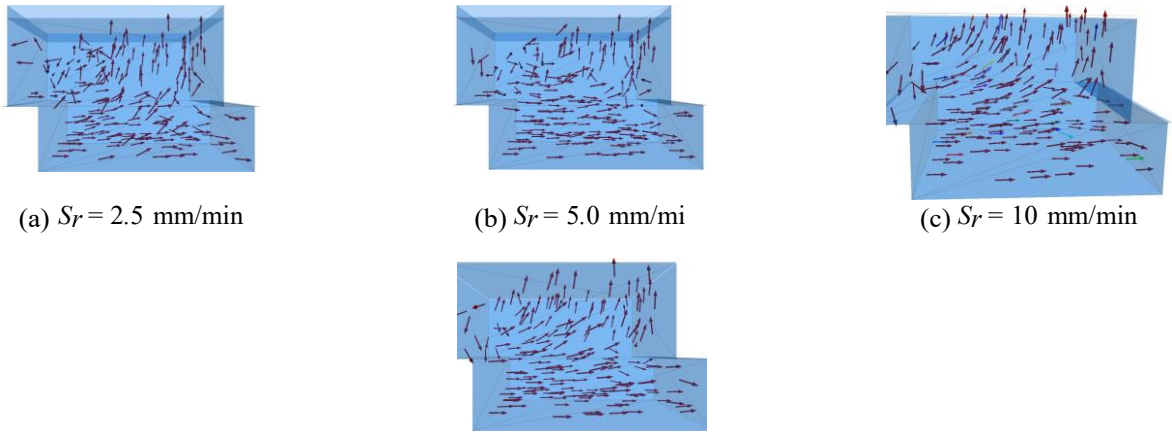

(a) $Sr = 2.5$ mm/min (b) $Sr = 5.0$ mm/mi (c) $Sr = 10$ mm/min

(d) $Sr = 20$ mm/min

Fig. 10 Ballast particle displacement at 45 mm shear displacement for four shearing rate

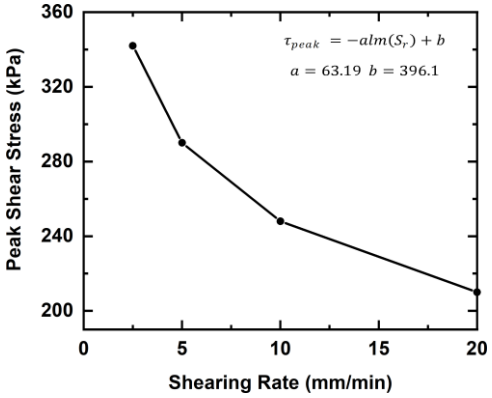


Fig. 11 Variation of peak shear stress with shearing rate

breakage happens at high shearing rates. According to Fig. 9, the shearing rate also causes an increase in the vertical displacement and decrease in dilation angle ($\psi$). As $S_r$ grows from 5 to 10 mm/min, the vertical displacement goes up from 25 to 27 mm. The dilation angle $\psi$ decreases from 25 to 18 as $S_r$ increases from 2.5 to 10 mm/min. Variation of $\psi$ with $S_r$ is expressed in Eq. (2) as $ae^b(S_r)$, where $a$ and $b$ are empirical constants. The value of relevant constants is shown in Fig. 12. This attribute to train with high speed results in more vertical and lateral deformation.

As the shearing rate rises, the friction angle ($\phi$) decreases, as seen in Fig. 13. The friction angle decreases from 78 to 71 and empirical expression in Eq. (3) for it. The values of relevant empirical constant $a$ and $b$ is indicated in Fig. 13. These expressions can be used to forecast related items. These expressions can be used to predict related entities.

$$\tau_{\text{peak}} = -a \ln(S_r) + b \tag{1}$$

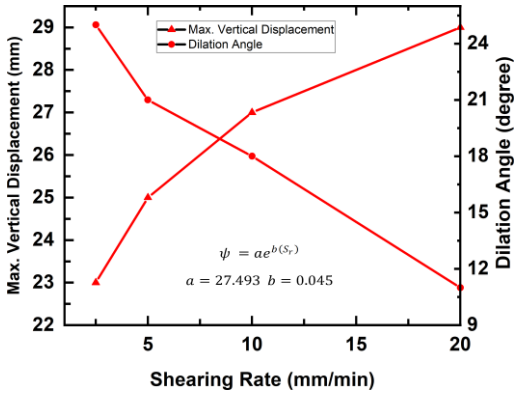


Fig. 12 Influence of shearing rate on dilation of ballast assembly

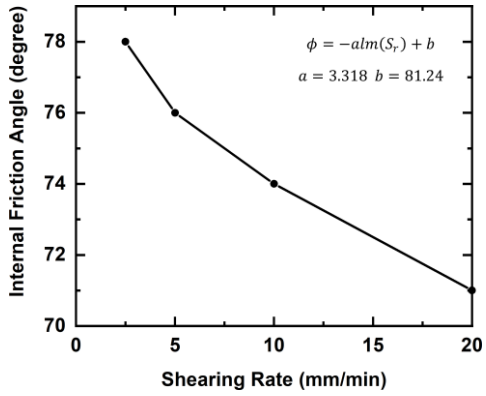


Fig. 13 Influence of shearing rate on friction angle ($\phi$) of ballast assembly

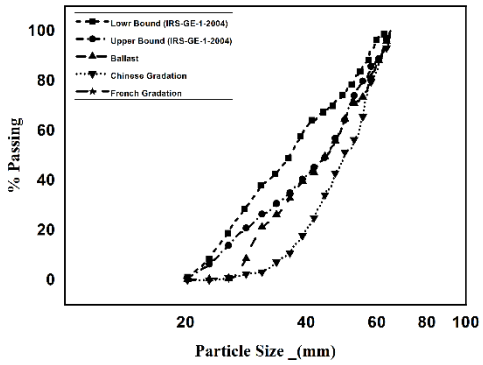


Fig. 14 Particle size distribution

$$\psi = ae^{b(Sr)} \tag{2}$$

$$\phi = -a\ln(S_r) + b \tag{3}$$

## 5. Influence of PSD

It is a well-known fact that different grading of granular material exhibits distinct mechanical behaviour. Very few literature are available on the effects of the PSD of ballast

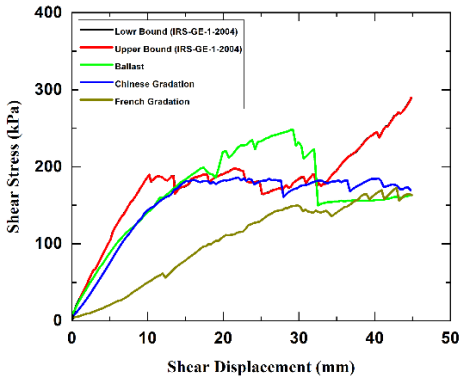


Fig. 15 Influence of PSD on shear behaviour of ballast assembly

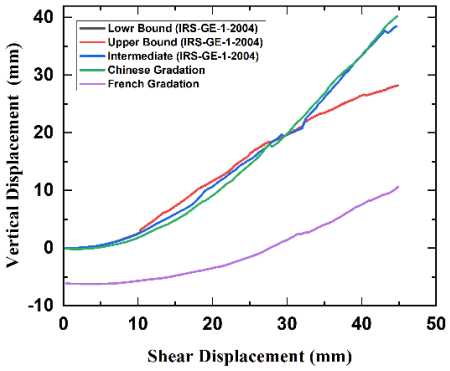


Fig. 16 Influence of PSD on dilation behaviour of ballast assembly

particles on its shear behaviour. Many researchers have investigated the grading effects of soil and pavement aggregate such as Hamidi *et al.* (2012), Salazar *et al.* (2015), Wang and Arson (2016). In this study, five different gradations are simulated in DEM to evaluate the effect of PSD on ballast shear behaviour. Three different PSDs are simulated in DEM as per IRS-GE-1-2004. Lower bound gradation, upper bound gradation and a gradation be- tween lower and upper bound limit of Indian railway ballast specification (IRS-GE-1 (2004) are simulated. China HSR ballast gradation Zhang *et al.* (2017) and France gradation In draratna *et al.* (2011b) are also simulated in this study. Fig. 14 shows these five PSD. The simulated Indian ballast gradations range from broad to moderate. While the Chinese HSR and French gradations are uniformly graded. Table 3 presents the characteristics of these five PSD.

Fig. 15 shows variation of shear stress with shear displacement for these five PSD. The shear and mechanical behaviour of these five gradations of ballast assembly are reflected in this plot. The upper bound gradation for IRS-GE-1-2004 is broader gradation as compare to lower bound gradation.

The upper bound has higher peak strength than lower bound gradation. Broader gradation has a larger range of plastic deformation. The permanent strain is much more in broader gradation. Both the lower and upper bounds of the Indian gradation have the same elastic stiffness, but the degree of permanent strain is substantially greater in the upper

Table 3 Characteristics of different gradations

| **PSD** | $D_{10}(mm)$ | $D_{30}$ (mm) | $D_{60}$ (mm) | $D_{max}$ (mm) | $D_{min}$ (mm) | $C_u$ | $C_c$ |
|---|---|---|---|---|---|---|---|
| China HSR gradation | 36 | 43 | 54 | 65 | 20 | 1.5 | 0.95 |
| Indian gradation lower bound | 23 | 28 | 39 | 63 | 20 | 1.7 | 0.87 |
| Indian gradation intermediate bound | 24 | 33 | 49 | 65 | 20 | 2 | 0.03 |
| Indian gradation upper bound | 28 | 35 | 49 | 65 | 20 | 1.75 | 0.89 |
| French gradation | 30 | 35 | 45 | 63 | 25 | 1.5 | 0.90 |

Table 4 Characteristics of five simulated gradations

| Gradation | Peak shearstress (kPa) | Max. vertical displacement (mm) | Peak dilationangle (degree) |
|---|---|---|---|
| China HSR | 184 | 40.2 | 28 |
| Indian lower bound | 189 | 28 | 24 |
| Indian intermediate bound | 248 | 38.5 | 27 |
| Indian upper bound | 285 | 28.2 | 18 |
| French | 172 | 10.6 | 10 |

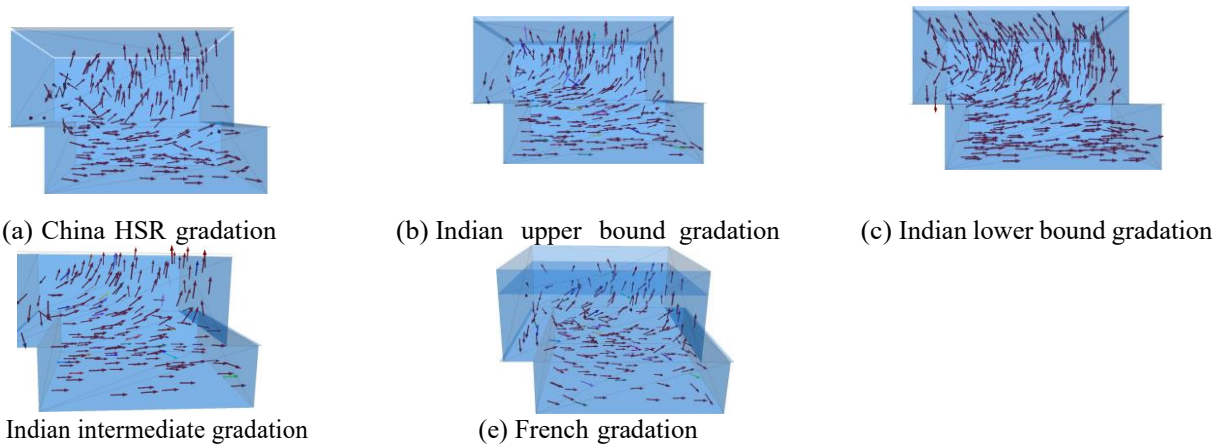

(a) China HSR gradation (b) Indian upper bound gradation (c) Indian lower bound gradation

(d) Indian intermediate gradation (e) French gradation

Fig. 17 Ballast particle displacement at 45 mm shear displacement for five gradations

bound. The Intermediate simulated gradation of IRS: GE:1:2004 IRS-GE-1 (2004) has higher elastic stiffness and larger permanent strain than the other two simulated Indian ballast gradations. It means broader gradations have better strength than uniform gradation. Chinese HSR gradation and French gradation are also uniformly graded. The Chinese HSR gradation has a higher strength and elastic stiffness than the French gradation. Chinese HSR gradation has larger plastic deformation than French gradation. For Chinese HSR gradation, plastic deformation begins early at small shear displacement. The increased plastic deformation and consequently large permanent strain produces a fall in peak strength, resulting in low strength in uniform gradation. As demonstrated in Fig. 17, the shearing operation causes in all five gradations to compress at first.. The amount of contraction is more for uniform gradations as compared to moderately and broadly graded ballast.

It is observed that uniformly graded PSD have less strength and dilation. Among these five PSD Chinese HSR gradation has highest value of dilation angle as well vertical displace- ment. The higher dilation leads to less breakage of ballast. French gradation shows a very small dilation among all five gradations. The amount of displacement is only 10 mm and dilation angle is 10.

## 6. Effects of shear box size and shape

In this study, four square cross section shear boxes of size 200 mm × 200 mm, 300 mm× 300 mm and 450 mm × 450 mm are modelled. One rectangular cross section shear box of size 300 mm × 200 mm is also modeled.

Fig. 18 presents variation of shear stress for different sizes of shear box. The peak shear strength increases with decreasing size of the shear box. The peak shear strength decreases from 997 kPa to 115 kPa as shear box area decreases from 200 × 200 $mm^2$ to 450 × 450 $mm^2$. The peak shear strength of the smaller shear box is the highest, which is consistent with the previous laboratory results. The square cross-section shear box has been found to have more accurate peak shear strength than the rectangular cross-section shear box. The cause of this phenomena is larger

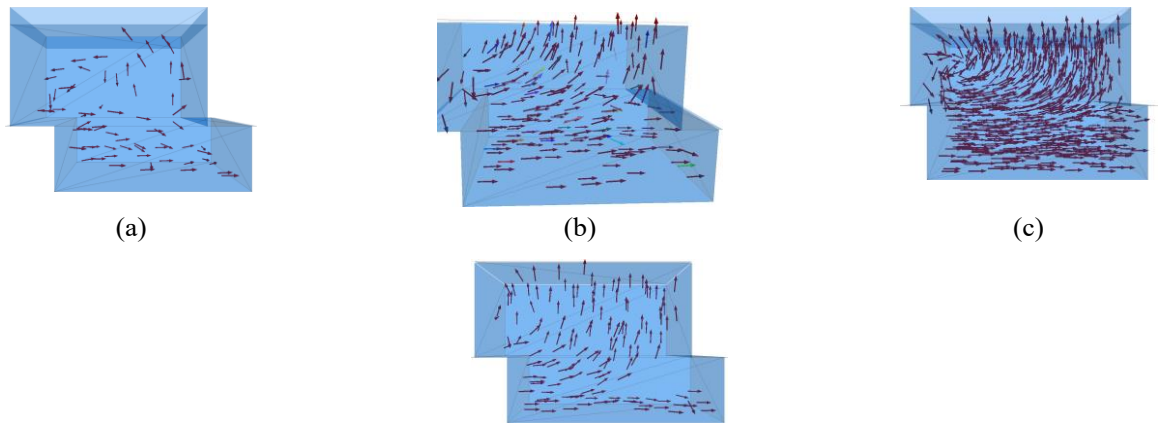

(a) (b) (c)

(d)

Fig. 20 Dilation behaviour of ballast at 45 mm shear displacement for different shear box size and shape (a) 200 × 200 $mm^2$ (b) 300 × 300 $mm^2$ (c) 450 × 450 $mm^2$ (d) 300 × 200 $mm^2$

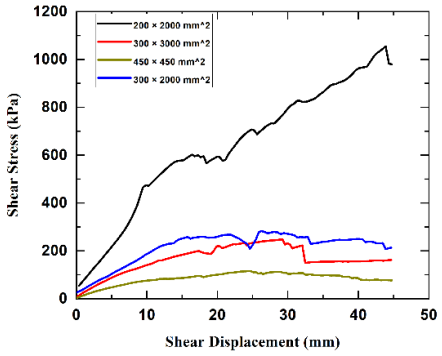


Fig. 18 Influence of shear box size and shape

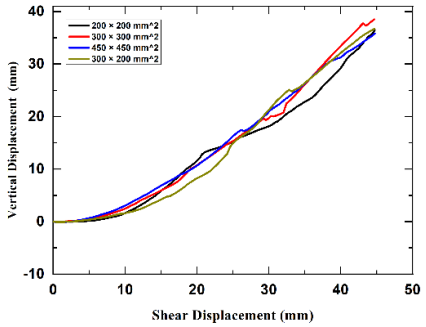


Fig. 19 Influence of shear box size and shape on dilation behaviour of ballast assembly

loading plate area and less ballast particle mobilisation. It is observed that in the larger-sized shear box, particle concentration and upward movement in the upper box is much higher than in the lower box. It is observed that the stiffness of assembly of particles decreases with increasing size of the shear box. Rectangular cross-section shear box has almost accurate stiffness of assembly of particles. At the initial stage of shearing, the upward movement of particles shows dilation in the larger-sized shear box. However, in the smaller and rectangular shear box, the particle assembly contracts first, then dilate as the upward movement causes the assembly to expand; as shown in Fig. 20. It has been observed that the amount of vertical displacement and dilation are not so much affected with size and shape of shear box. The shear zone thickness is also found to increase with increase in shear box size. Fig. 21 presents distribution of contact force for shear boxes at 45 mm shear displacement. Contact forces are plotted as arrow, whose direction shows action of contact forces between particles. It illustrates the transmission of applied load within the particle assembly. Initially contact forces were uniformly distributed throughout assembly. Contact forces are intensified from bottom-left to top-right portion of shear box. Accumulation and intensity of contact forces increases with size of shear box. No. of contacts increases and contact force decreases with increasing shear box size as indicated in Figs. 21(a)-21(d). This can be attributed to change in coordination number and reduction in shear stress with increasing shear box size.

## 7. Conclusions

This study explores railway ballast behavior at a microscopic scale through direct shear testing using DEM simulations. By modeling irregular shape clumps, the micromechanical properties of ballast particles are analyzed, considering factors like shape, size, PSD, and shear box dimensions. In the present study, the DEM simulation shows good agreement with previous research findings. Notably, the applied normal stress, shearing rate, and specimen size significantly influenced the shear strength, friction angle, and dilation of ballast. The friction angle ($\phi$) of ballast nonlinearly decreases with rising normal stress and shearing rate. The dilation angle ($\Psi$) decreases from 25° to 18° as the shearing rate increases from 2.5 to 10 mm/min. With increase in shearing rate, a substantial number of ballast move upward, leading to a decrease in coordination number and shear strength of ballast assembly. Re- garding

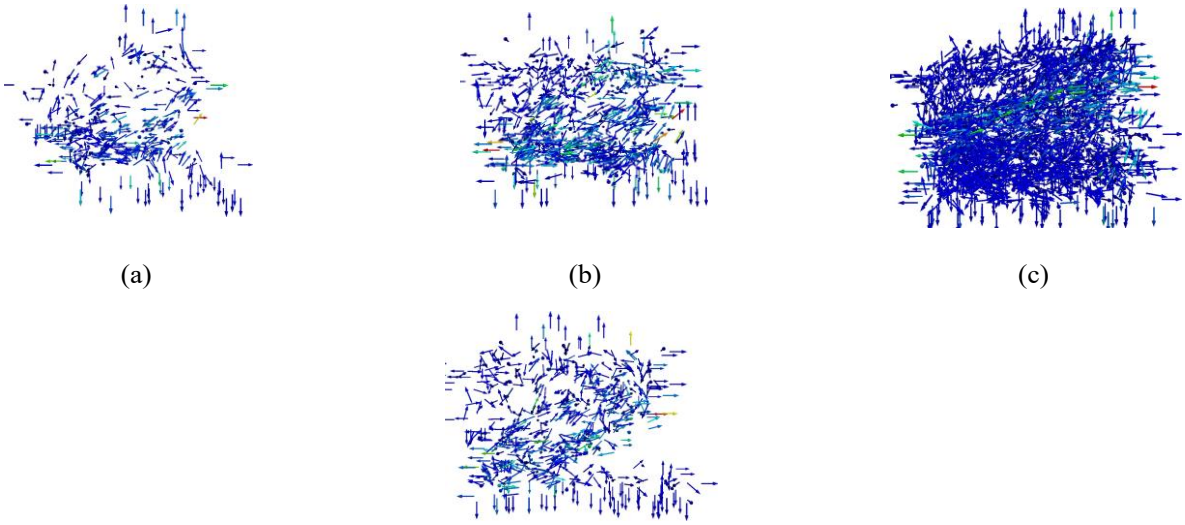

(a) (b) (c)

(d)

Fig. 21 Distribution of contact forces at 45 mm shear displacement for different shear box size and shape (a) 200 × 200 $mm^2$ (b) 300 × 300 $mm^2$ (c) 450 × 450 $mm^2$ (d) 300 × 200 $mm^2$

gradations, the intermediate simulated gradation of the Indian ballast specification exhibits higher elastic stiffness and greater plastic deformation compared to the other two simulated PSDs of Indian ballast specification. Among these gradations, China HSR grada- tion displays the highest dilation angle, while the French gradation exhibits the lowest shear strength and dilation angle. Furthermore, the peak shear stress rises with decreasing shear box size, while the accumulation and intensity of contact force increase with larger shear box sizes. This results in a higher number of contacts and lower contact force values with the increase in shear box size.

## References


Alam, M.N. and Hussaini, S.K.K. (2023), "Performance of geogrid-reinforced rubber-coated ballast and natural ballast mix under direct shear conditions", *J. Mater. Civil Eng*., **35**(9), 04023290. https://doi.org/10.1061/JMCEE7.MTENG-15461.

Bolton, M. (1986), "The strength and dilatancy of sands", *Geotechnique*, **36**(1), 65-78. https://doi.org/10.1680/geot.1986.36.1.65P.

Carroll, M.D. (1979), *Sample size effects using the NGI direct simple shear apparatus*, Technical report, Defense Technical Information Center, VA.

Cerato, A.B. and Lutenegger, A.J. (2006), "Specimen size and scale effects of direct shear box tests of sands", *Geotech.Test. J*., 29(6), 507-516. https://doi.org/10.3923/jas.2010. 2027.2033.

Cui, L. and O'sullivan, C. (2006), "Exploring the macro-and micro-scale response of an idealised granular material in the direct shear apparatus", *Geotechnique*, **56**(7), 455-468. https://doi.org/10.1680/geot.2006.56.7.455.

Cundall, P.A. and Strack, O.D. (1979), "A discrete numerical model for granular assemblies", *Geotechnique*, **29**(1), 47-65. https://doi.org/10.1680/geot.1979.29.1.47.

Dadkhah, R., Ghafoori, M., Ajalloeian, R. and Lashkaripour, G.R. (2010), "The effect of scale direct shear tests on the strength parameters of clayey sand in Isfahan city, Iran", *J. Appl. Sci.*, **18**, https:doi.org/10.3923/jas.2010.2027.2033.

Fu, Q. and Wu, Y. (2019), "Three-dimensional finite element modelling and dynamic response analysis of track-embankment-ground system subjected to high-speed train moving loads", *Geomech. Eng*., **19**(3), 241-254. https://doi.org/10.12989/gae.2019.19.3.241.

Gong, J., Li, L., Zhao, L., Zou, J. and Nie, Z. (2021), "DEM study on effects of fabric and aspect ratio on small strain stiffness of granular soils", *Geomech. Eng*., **24**(1), 57-65. https://doi.org/10.12989/gae.2021.24.1.057.

Hamidi, A., Azini, E. and Masoudi, B. (2012), "Impact of gradation on the shear strength-dilation behavior of well graded sand-gravel mixtures", *Scientia Iranica*, **19**(3), 393-402. http://doi. org/10.1007/s10035-004-0189-3.

Huang, H. and Tutumluer, E. (2011), "Discrete element modeling for fouled railroad ballast", *Constr. Build. Mater*., **25**(8), 3306-3312. https://doi.org/10.1016/j.conbuildmat. 2011.03.019.

Huang, H. and Tutumluer, E. (2014), "Image-aided element shape generation method in discrete- element modeling for railroad ballast", *J. Mater. Civil Eng*., **26**(3), 527-535. https://doi.org/10.1061/(ASCE)MT.1943-5533.0000839.

Huang, H., Tutumluer, E. and Dombrow, W. (2009a), "Laboratory characterization of fouled railroad ballast behavior", *Transport. Res. Record*, **2117**(1), 93-101, https://doi.org/10.3141/ 2117-1.

Huang, H., Tutumluer, E., Hashash, Y.M. and Ghaboussi, J. (2009b), "Discrete element modeling of aggregate behavior in fouled railroad ballast", in "Recent Advancement in Soil Behavior, in Situ Test Methods, Pile Foundations, and Tunneling: Selected Papers from the 2009 GeoHunan International Conference", 33-41, https://doi.org/10.1061/41044(351)6.

Indraratna, B., Hussaini, S.K.K. and Vinod, J. (2013), "The lateral displacement response of geogrid- reinforced ballast under cyclic loading", *Geotext. Geomembranes*, **39**, 20-29. https://doi.org/10.1016/j.geotexmem.2013.07.007.

Indraratna, B., Ngo, N.T. and Rujikiatkamjorn, C. (2011a), "Behavior of geogrid-reinforced ballast under various levels of fouling", *Geotext. Geomembranes*, **29**(3), 313-322, https://doi.org/10.1016/j.geotexmem.2011.01.015.

Indraratna, B., Ngo, N.T., Rujikiatkamjorn, C. and Vinod, J. (2014), "Behavior of fresh and fouled railway ballast subjected to direct shear testing: discrete element simulation", *Int. J.*

*Geomech*., **14**(1), 34-44, https://doi.org/10.1061/(ASCE)GM.1943-5622.0000264.
Indraratna, B., Salim, W. and Rujikiatkamjorn, C. (2011b), Advanced rail geotechnology-ballasted track, CRC press. https://doi.org/10.1201/b10861.
IRS-GE-1 (2004), "Specification for track ballast", Research Design and Standard organisation (RDSO).
Itasca, C. (2017), "PFC3D v5. 0-user manual", Itasca Consulting Group, Minneapolis.
Jewell, R. (1989), "Direct shear tests on sand", *Geotechnique*, **39**(2), 309-322. https://doi.org/ 10.1680/geot.1989.39.2.309.
Lim, W. and McDowell, G. (2005), "Discrete element modelling of railway ballast", *Granular. Matter.*, 7(1), 19-29. https://doi.org/10.1007/s10035-004-0189-3.
Liu, X., Zhou, A., Shen, S.L., Li, J. and Arulrajah, A. (2021), "Modelling unsaturated soil-structure interfacial behavior by using DEM", *Comput. Geotech*., **137**, 104305, https://doi.org/10.1016/j.compgeo.2021.104305.
Lu, M. and McDowell, G. (2007), "The importance of modelling ballast particle shape in the discrete element method", *Granular. Matter.*, **9**(1-2), 69. https://doi.org/10.1007/s10035-006-0021-3.
Masson, S. and Martinez, J. (2001), "Micromechanical analysis of the shear behavior of a granular material", *J. Eng. Mech*., **127**(10), 1007-1016. https://doi.org/:10.1061/(ASCE)0733-9399(2001)127:10(1007).
McDowell, G., Harireche, O., Konietzky, H., Brown, S. and Thom, N. (2006), "Discrete element modelling of geogrid-reinforced aggregates", *Proceedings of the Institution of Civil Engineers-Geotechnical Engineering*, **159**(1), 35-48. https://doi.org/10.1680/geng.2006.159.1.35.
Mikasa, M. (1960), "New direct shear test apparatus", *Proceedings of the 5th Annual Meeting, JSCE*, 45-48.
Ngamkhanong, C., Kaewunruen, S. and Baniotopoulos, C. (2017), "A review on modelling and monitoring of railway ballast", *Struct. Monit. Maintenance*, **4**(3), 195. https://doi.org/10.12989/smm.2017.4.3.195.
Ngo, N.T., Indraratna, B. and Rujikiatkamjorn, C. (2014), "DEM simulation of the behaviour of geogrid stabilised ballast fouled with coal", *Comput. Geotech*., **55**, 224-231. https://doi.org/10.1016/j.compgeo.2013.09.008.
Oda, M. and Iwashita, K. (2020), Mechanics of granular materials: an introduction, CRC press. https://doi.org/10.1201/9781003077817.
Palmeira, E. and Milligan, G. (1991), "Scale effects in direct shear tests on sand", **28**, 340.
Parsons, J.D. (1936), "Progress report on an investigation of the shearing resistance of cohesion- less soils", *Proceedings of the 1st international conference on soil mechanics and foundation engineering*.
Salazar, A., S´aez, E. and Pardo, G. (2015), "Modeling the direct shear test of a coarse sand using the 3D discrete element method with a rolling friction model", *Comput. Geotech*., **67**, 83-93. https://doi.org/10.1016/j.compgeo.2015.02.017.
Shibuya, S., Mitachi, T. and Tamate, S. (1997), "Interpretation of direct shear box testing of sands as quasi-simple shear", *Geotechnique* **47**(4), 769-790. https://doi.org/10.1680/geot.1997.47.4.769.
Suhr, B., Marschnig, S. and Six, K. (2018), "Comparison of two different types of railway ballast in compression and direct shear tests: experimental results and DEM model validation", *Granular. Matter.*, **20**(4), 1-13. https://doi.org/10.1007/s10035-018-0843-9.
Suhr, B. and Six, K. (2016), "On the effect of stress dependent interparticle friction in direct shear tests", *Powder Technol.*, **294**, 211-220. https://doi.org/10.1016/j.powtec.2016.02.029.
Suhr, B. and Six, K. (2017), "Parametrisation of a DEM model for railway ballast under different load cases", *Granular. Matter*., **19**(4), 1-16. https://doi.org/10.1007/s10035-017-0740-7.
Sweta, K. and Hussaini, S.K.K. (2018), "Effect of shearing rate on the behavior of geogrid-reinforced railroad ballast under direct shear conditions", *Geotext. Geomembranes*, **46**(3), 251-256. https://doi.org/10.1016/j.geotexmem.2017.12.001.
Sweta, K. and Hussaini, S.K.K. (2019), "Performance of the geogrid-reinforced railroad ballast in direct shear mode", *Proceedings of the Institution of Civil Engineers-Ground Improvement*, **172**(4), 244-256, URL https://doi.org/10.1680/jgrim.18.00107.
Tsoungui, O., Vallet, D. and Charmet, J.C. (1999), "Numerical model of crushing of grains inside two-dimensional granular materials", *Powder Technol.*, **105**(1-3), 190-198. https://doi.org/10.1016/S0032-5910(99)00137-0
Wang, P. and Arson, C. (2016), "Discrete element modeling of shielding and size effects during single particle crushing", *Comput. Geotech.*, **78**, 227-236, https://doi.org/10.1016/j.compgeo.2016.04.003.
Wang, Z., Jing, G., Yu, Q. and Yin, H. (2015), "Analysis of ballast direct shear tests by discrete element method under different normal stress", *Measurement*, **63**, 17-24. https://doi.org/10.1016/j.measurement.2014.11.012.
Wu, P.K., Matsushima, K. and Tatsuoka, F. (2008), "Effects of specimen size and some other factors on the strength and deformation of granular soil in direct shear tests", *Geotech. Test. J*., **31**(1), 45-64. https://doi.org/10.1520/GTJ100773.
Zahran, K. and Naggar, H.E. (2020), "Effect of sample size on TDA shear strength parameters in direct shear tests", *Transport. Res. Record*, **2674**(9), 1110-1119. https://doi.org/10.1177/0361198120934482.
Zhang, X., Zhao, C. and Zhai, W. (2017), "Dynamic behavior analysis of high-speed railway ballast under moving vehicle loads using discrete element method", *Int. J. Geomech*., **17**(7), 04016157. https://doi.org/10.1061/(ASCE)GM.1943-5622.0000871.

*GC*